

## Study of the Structural, Optical, and Morphological Properties of SnO<sub>2</sub> Nanofilms Under the Influence of Gamma Rays

**Ola Mohammed Firas<sup>1a\*</sup> and Basim Khalaf Rejah<sup>1b</sup>**

<sup>1</sup>*Department of Physics, College of Science for Women, University of Baghdad, Baghdad, Iraq*

<sup>b</sup>E-mail: [basimkr\\_phys@csw.uobaghdad.edu.iq](mailto:basimkr_phys@csw.uobaghdad.edu.iq)

<sup>a\*</sup>Corresponding author: [Ula.Abdullah1604@csw.uobaghdad.edu.iq](mailto:Ula.Abdullah1604@csw.uobaghdad.edu.iq)

### Abstract

This study reports the fabrication of tin oxide (SnO<sub>2</sub>) thin films using pulsed laser deposition (PLD). The effect of <sup>60</sup>Co (300, 900, and 1200 Gy) gamma radiation on the structural, morphological, and optical features is systematically demonstrated using X-ray diffraction (XRD), field emission scanning electron microscopy (FE-SEM), atomic force microscopy (AFM), and ultraviolet-visible light analysis (UV-Vis), respectively. In XRD tests, the size of the crystallites decreased from 45.5 to 40.8 nm for the control samples and from 1200 Gy to <sup>60</sup>Co for the irradiated samples. Using FESEM analysis, the particle diameter revealed a similar trend to that attained using XRD; in particular, the average diameters were 93.8 and 79.9 nm for the samples mentioned above. A similar profile was observed for the AFM analysis in which an increase in the radiation dose from 300 to 1200 Gy resulted in a decrease in the RMS values from 74.6 to 32.25 nm. Contrariwise, the calculated optical band gap demonstrated an increasing profile where optical band gaps of 3.08 and 3.18 eV were acquired for control and samples irradiated with 900 Gy. However, the attained optical band gap was further increased to 3.24 eV due to the <sup>60</sup>Co gamma radiation increment to 1200 Gy.

### Article Info.

#### Keywords:

*SnO<sub>2</sub>, gamma radiation, pulsed laser, deposition, properties.*

#### Article history:

Received: May 11, 2023

Revised: Jun. 21, 2023

Accepted: Jul. 09, 2023

Published: Sep.01, 2023

### 1. Introduction

Owing to the great potential applications of metal oxide nanoparticles in various fields, the alteration of their physical characteristics is considered of pronounced importance within research society. Metal oxide semiconductors, particularly, are well-known for their attractive magnetic, electrical, and optical characteristics [1-5]. Furthermore, these physical characteristics of metal oxide semiconductors, structural, optical, electrical, etc., are significantly altered upon exposure to ionizing radiation, particularly gamma radiation [6-10]. Herein, it is noteworthy to mention that gamma radiation excessively influences the addressed characteristics. These changes depend on the irradiation dosage as well as the sensibility of the solid-thin film towards specific radiation [11-16]. In detail, when gamma radiations with adequate energy level interact with metal oxide semiconductor, ionization and atomic disorientation occurs. Continuously, gamma irradiation of metal oxide semiconductors results in lattice defects production; for example, dislocation loops and defects clusters near the metal/oxide interface [17-23]. These drawbacks may, in turn, lead to low device performance in the target application, such as optical communication devices, solar cells, photodetectors, light-emitting diodes, and optical dosimeters [24-28]. Therefore, a sound investigation of the addressed damages and their effects on the physical characteristics is being well-inspected on several metal oxide semiconductors. Among different metal oxide semiconductors, tin oxide (SnO<sub>2</sub>) nanoparticle is an n-type semiconductor with a wide energy band gap (3.6 eV) and high chemical and mechanical stability [29-31]. Such properties allow SnO<sub>2</sub> to be of great interest in many

applications, such as liquid crystal displays, far-infrared detectors, heat-reflecting mirrors, solid-state gas sensors, and optoelectronic devices [32-35].

This study reports the effect of  $^{60}\text{Co}$  gamma radiation (300, 900, and 1200 Gy) on the structural, morphological, and optical characteristics of  $\text{SnO}_2$  nanofilm deposited using the pulsed laser deposition technique (PLD). Further, the stated characteristics are examined as a function of the utilized dose range.

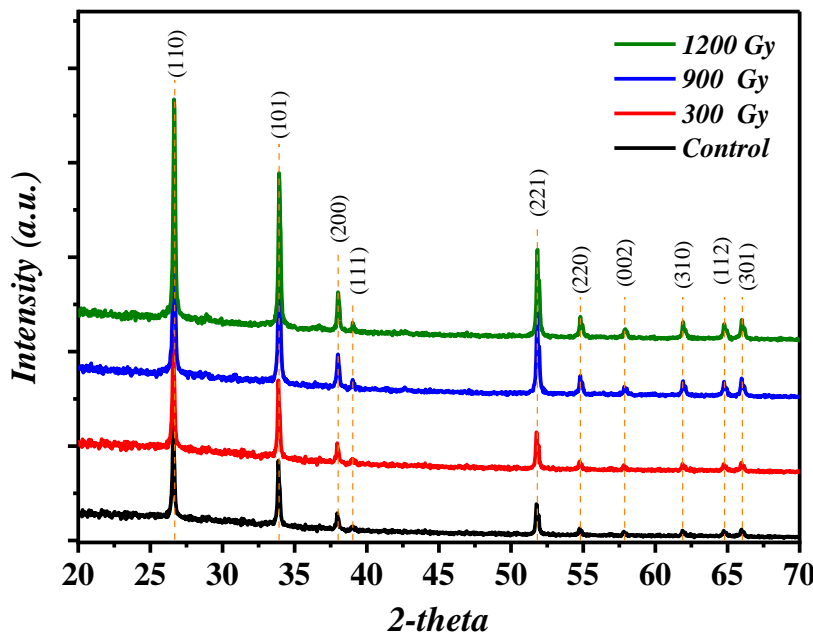
## 2. Experimental Work

Deposition of  $\text{SnO}_2$  nanofilms was achieved via the well-established pulsed laser deposition technique on glass substrates under a high-vacuum environment; the glass substrates were subjected to a multi-cycle washing process using soppy water, ethanol, and acetone, respectively. The  $\text{SnO}_2$  powder was mechanically pressed under 5 tons for 20 minutes to obtain the deposition target. Prior to each deposition process, the chamber within which the deposition took place was evacuated and heated to remove any possible water vapor and/or contaminants. Subsequently, the glass substrate was placed vertically at a 10 cm from the utilized  $\text{SnO}_2$  target. Herein, the  $\text{SnO}_2$  target was exposed to Nd:YAG laser with a wavelength of 1064 nm and energy of 300 mJ, while the number of pulses and repetition rate were 60 pulses and 6 Hz, respectively. After this, the attained  $\text{SnO}_2$  nanofilms were exposed to different gamma ray doses (300, 900, and 1200 Gy) using a  $^{60}\text{Co}$  gamma radiation source of 12 Gy/hr dose rate under air atmosphere and room temperature.

## 3. Results and Discussion

The XRD patterns of the deposited control and  $^{60}\text{Co}$  irradiated (300, 900, and 1200 Gy)  $\text{SnO}_2$  films are illustrated in Fig.1. Specifically, diffraction peaks were attained at around  $26.6^\circ$ ,  $33.9^\circ$ ,  $37.8^\circ$ ,  $39.0^\circ$ ,  $51.8^\circ$ ,  $54.8^\circ$ ,  $54.8^\circ$ ,  $57.8^\circ$ ,  $61.9^\circ$ ,  $64.8^\circ$  and  $66.0^\circ$  corresponding to the  $\text{SnO}_2$  crystal formation planes (110), (101), (200), (111), (221), (220), (002), (310), (112), and (301), respectively; such crystal orientations were found to be in accordance with the Joint Committee on Powder Diffraction Standards (JCPDS 85-0712). The acquired results were in good agreement with previously published reports [36-38]. It should be mentioned that the resultant peak intensity of (110) increased with the increase of the gamma dose. Interestingly, the calculated crystallite size at (110) using Debye-Scherrer equation indicated smaller size as a function of dose increment (Table 1) [39]. Particularly, the control sample (control) exhibited a crystallite size of 45.5 nm; samples irradiated at 300, 900, and 1200 Gy demonstrated sizes of 44.5, 41.2, and 40.8 nm, respectively. On the other hand, the full-width at half maximum (FWHM) showed an inverse behavior wherein high gamma dose resulted in low crystallinity. This could be mainly because higher gamma radiation dose rearranged the lattice nanostructure [10, 40, 41].

Fig. 2 (a-d) elucidates the FE-SEM topographies of the deposited control and  $^{60}\text{Co}$  irradiated (300, 900, and 1200 Gy)  $\text{SnO}_2$  films, wherein all deposited samples, with respect to the radiation statuses, revealed well-compacted surfaces. It can be observed that the deposited particles have obvious agglomeration conduct. However, such a singularity was less noticed at higher irradiation doses, 900 Gy and above. Further, the estimated average nanoparticle diameters decreased as the irradiation dose increased. In detail, control  $\text{SnO}_2$  demonstrated an average diameter of 93.8 nm (Fig. 2, a), while the irradiated nanoparticle diameters were found to be 86.9, 82.4, and 79.7 nm for irradiation doses of 300, 900, and 1200 Gy, respectively. Therefore, it can be concluded, that the applied gamma radiation resulted in lowering the nanoparticle diameter.

Figure 1: XRD patterns of control and  $^{60}\text{Co}$  irradiated  $\text{SnO}_2$  films.Table 1: In-depth XRD parameters of the deposited  $\text{SnO}_2$  films at  $26.6^\circ$  (110).

Sample	2-theta (deg.)	FWHM	Crystallite size (nm)
Control	26.68	0.180	45.5
300 Gy	26.58	0.184	44.5
900 Gy	26.62	0.198	41.2
1200 Gy	26.64	0.200	40.8

The surface roughness and morphology of the deposited samples and the effect of Gamma irradiation were also investigated using the AFM technique. The AFM images are presented in Fig. 3 (a-d). The surface roughness of the control  $\text{SnO}_2$  films was found to be 52.6 nm while exposing  $\text{SnO}_2$  film to 300 Gy increased the surface roughness (60.9 nm). This was followed by enhanced surface roughness of 64.2 nm at 900 Gy before decreasing to 17.9 nm at 1200 Gy. The root mean square of the deposited  $\text{SnO}_2$  films was 61.9, 74.6, 87.82, and 32.25 nm for control and irradiated (300, 900, and 1200 Gy)  $\text{SnO}_2$  films, respectively. The AFM outcomes illustrate how the gamma dose increment could serve as a surface features indicator for this type of nanomaterial, wherein the applied gamma dose increment delivered higher values of surface roughness.

Fig. 4 elucidates the absorbance spectra of the control and  $^{60}\text{Co}$  irradiated (300, 900, and 1200 Gy)  $\text{SnO}_2$  films. A clear cut-off phenomenon is attained around 330 nm. This corresponds to the crystal formation of  $\text{SnO}_2$  nanoparticles. Further, a slight blue shift towards higher wavelength was noticed with the increase of the  $^{60}\text{Co}$  irradiation dose. The optical band gap, obtained using Tauc relation [42-44], is calculated according to Eq. (1) and demonstrated in Fig. 5.

$$\alpha h\nu = A(h\nu - E_g)^n \quad (1)$$

where:  $\alpha$  is the absorption coefficient,  $E_g$  is the average band gap of the material,  $n$  depends on the type of transition.

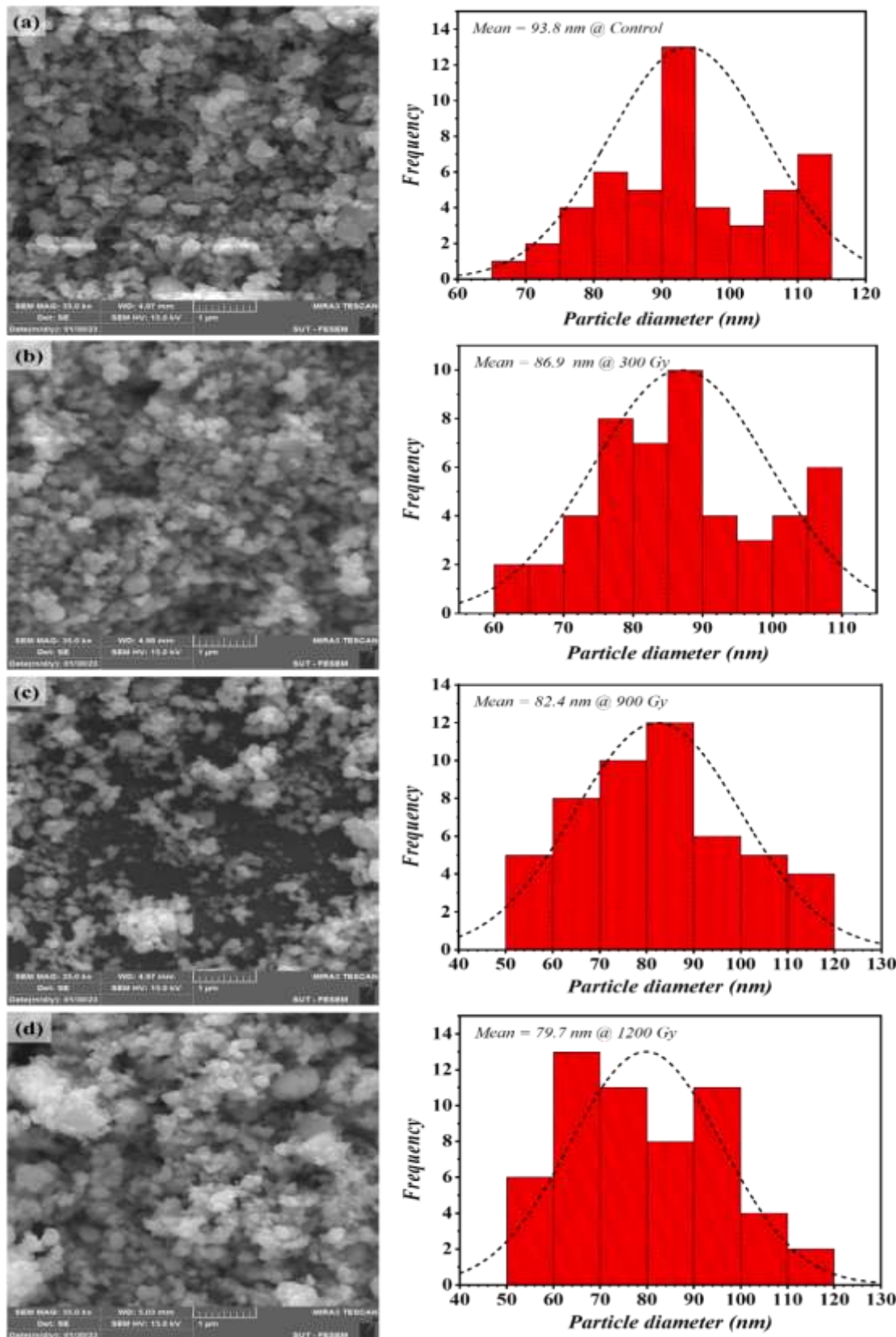
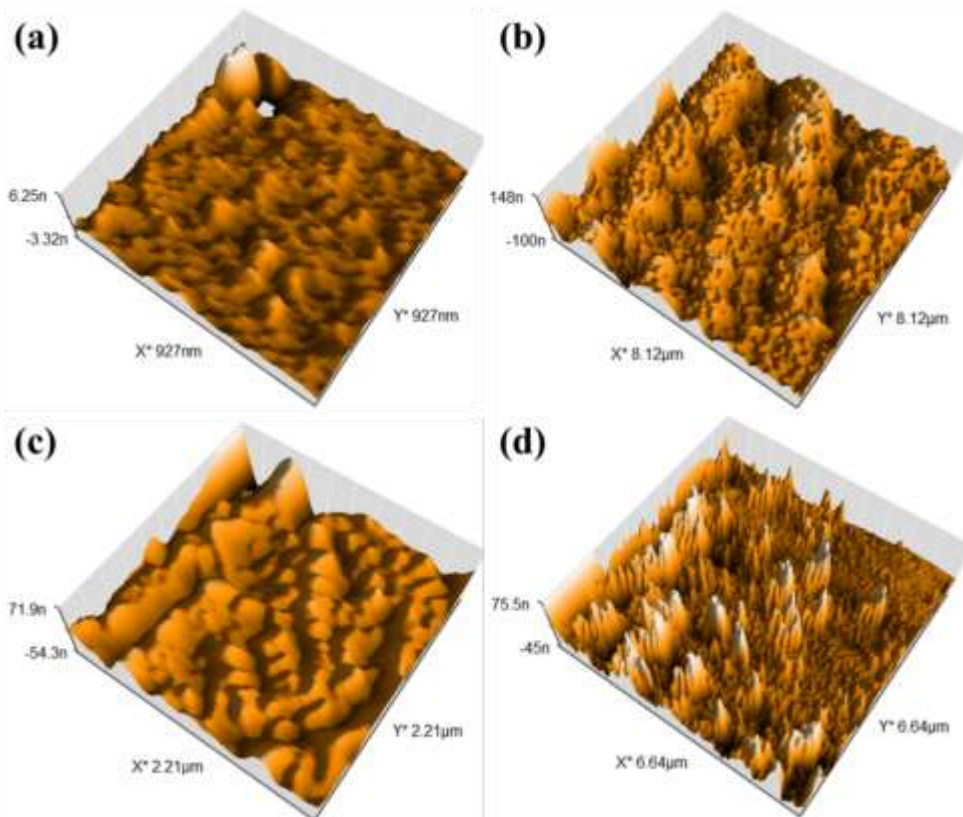
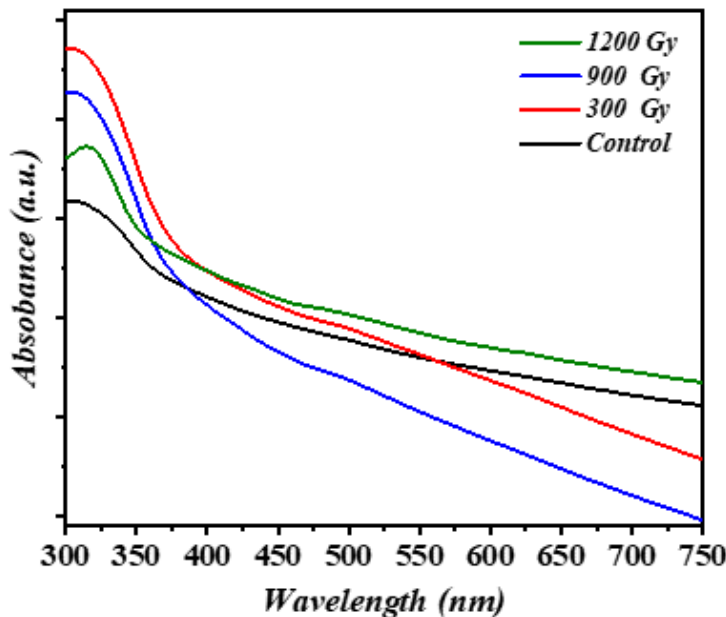


Figure 2: FE-SEM topographies of (a) control, (b) 300 Gy, (c) 900 Gy, and (d) 1200 Gy.



**Figure 3:** AFM images of (a) control  $\text{SnO}_2$ , (b) 300 Gy, (c) 900 Gy, and (d) 1200 Gy.



**Figure 4:** Absorbance spectra of control and  $^{60}\text{Co}$  irradiated  $\text{SnO}_2$ .

The control sample was with 3.08 eV optical band gap, whereas higher optical band gaps of 3.17 and 3.24 eV were noticed at higher gamma irradiation doses. The attained blue shift could be because of crystal defect and surface morphology changes, as the optical behavior of metal oxide depends on the surface roughness, defect, and crystal structure [45, 46]. The obtained results are in good agreement with previously published data [47-50].

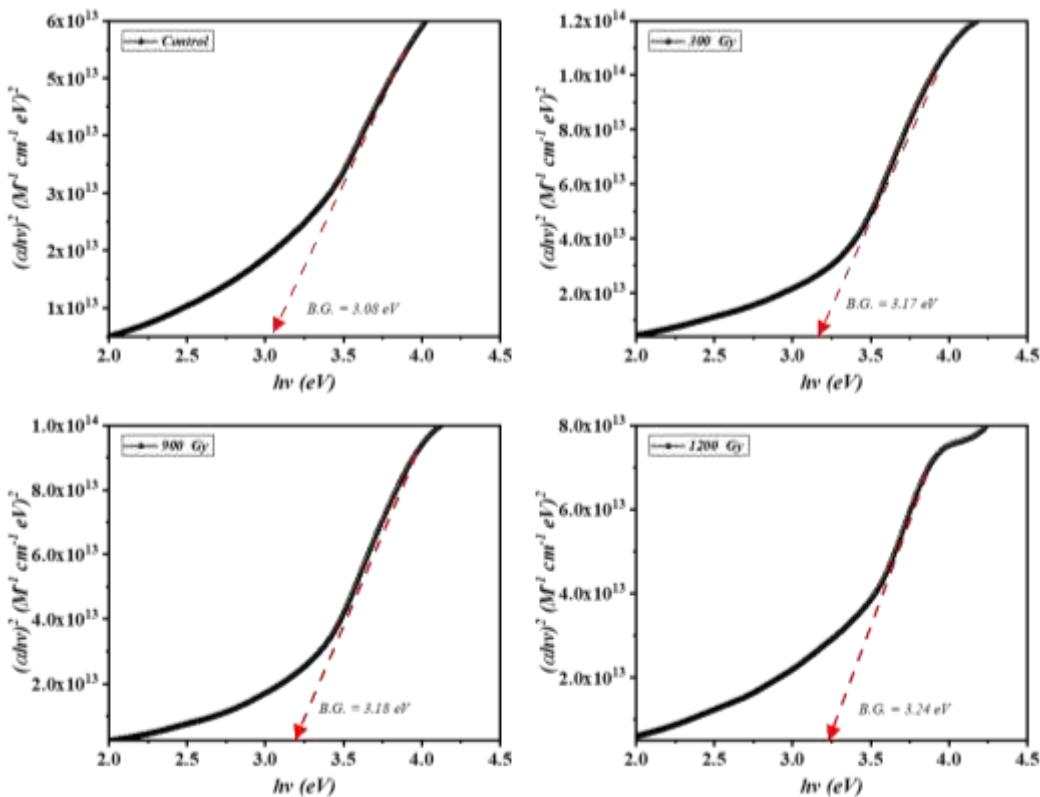


Figure 5: Optical band gap of control and  $^{60}\text{Co}$  irradiated  $\text{SnO}_2$  films.

#### 4. Conclusions

In conclusion, the deposited  $\text{SnO}_2$  using the pulsed laser deposition technique showed a noticeable response to applied gamma irradiation. This was perceived through the tests performed: XRD, FE-SEM, AFM, and UV-Vis. The applied gamma radiation showed a direct relationship to the deposited layers in terms of their properties. In detail, the crystallite size, particle diameter, and surface roughness demonstrated a proportional relationship to the applied gamma radiation doses. Particularly, the XRD analysis showed a decreasing trend in terms of the calculated crystallite size from 44.5 to 40.8 nm as the dose increased from 300 to 1200 Gy. In addition, a decrease from 86.9 to 76.7 nm in the attained nanoparticle diameters was perceived as the applied gamma radiation increased from 300 to 1200 Gy, respectively. Similarly, the investigated surface roughness increased from 52.6 to 64.2 nm upon increasing the applied radiation from 300 to 900 Gy. In contrast, the optical band gap, obtained from UV-Vis data, showed an inverse profile wherein a higher optical band gap was attained at higher gamma radiation doses; a value of 3.17 eV increased to 3.24 eV.

#### Acknowledgements

The authors would like to sincerely acknowledge the support provided by the University of Baghdad.

#### Conflict of interest

Authors declare that they have no conflict of interest.

#### References

1. E. Y. Salih, M. B. A. Bashir, A. H. Rajpar, I. A. Badruddin, and G. Bahmanrokh, Microelec. Engin. **258**, 111758 (2022).

2. F. Salleh, R. Usop, N. S. Saugi, E. Y. Salih, M. Mohamad, H. Ikeda, M. F. M. Sabri, M. K. Ahmad, and S. M. Said, *Appl. Surf. Sci.* **497**, 143736 (2019).
3. C. Sun, J. Yang, M. Xu, Y. Cui, W. Ren, J. Zhang, H. Zhao, and B. Liang, *Chem. Engin. J.* **427**, 131564 (2022).
4. A.-H. K. Iltaif, A. A. Jabor, R. H. Mukalaf, M. A. Abood, and F. G. Khalad, *Bagh. Sci. J.* **8**, 473 (2011).
5. M. B. A. Bashir, A. H. Rajpar, E. Y. Salih, and E. M. Ahmed, *Nanomat.* **13**, 802 (2023).
6. S. K. Sen, M. Noor, M. A. Al Mamun, M. S. Manir, M. Matin, M. Hakim, S. Nur, and S. Dutta, *Optic. Quant. Elect.* **51**, 1 (2019).
7. S. M. Ali, M. Algarawi, S. U.-D. Khan, and S. Aldawood, *Mater. Sci. Semicond. Proces.* **122**, 105474 (2021).
8. S. Yasmin and M. Sayyed, *Optik* **272**, 170218 (2023).
9. O. Agar, M. Sayyed, F. Akman, H. Tekin, and M. Kaçal, *Nucl. Engin. Tech.* **51**, 853 (2019).
10. R. Gupta, R. Kumar, R. Chauhan, and S. Chakarvarti, *Vacuum* **148**, 239 (2018).
11. A. Darwish, S. A. Issa, and M. El-Nahass, *Synth. Met.* **215**, 200 (2016).
12. A. Holmes-Siedle and L. Adams, *Handbook of Radiation Effects* (USA, Oxford University Press, 2002).
13. H. S. Isfahani, S. M. Abtahi, M. A. Roshanzamir, A. Shirani, and S. M. Hejazi, *Bull. Engin. Geo. Envir.* **78**, 4589 (2019).
14. S. A. Issa, M. Sayyed, M. Zaid, and K. Matori, *Resul. Phys.* **9**, 206 (2018).
15. K. Kaur, K. Singh, and V. Anand, *Nucl. Engin. Des.* **285**, 31 (2015).
16. A. Kumar, *Rad. Phys. Chem.* **136**, 50 (2017).
17. A. B. Selçuk, S. B. Ocak, and Ö. F. Yüksel, *Nucl. Instru. Meth. Phys. Res. Sec. A: Accel. Spectro. Detec. Assoc. Equip.* **594**, 395 (2008).
18. N. Lavanya, C. Sekar, A. Anithaa, N. Sudhan, K. Asokan, A. Bonavita, S. Leonardi, and G. Neri, *Nanotech.* **27**, 385502 (2016).
19. K. Abhirami, R. Sathyamoorthy, and K. Asokan, *Rad. Phys. Chem.* **91**, 35 (2013).
20. H. Wasly, A. El-Sadek, S. Elnobi, and A. A. Abuelwafa, *Euro. Phys. J. Plus* **137**, 1 (2022).
21. S. G. Khalil, M. A. Ameen, and N. J. Jubier, *Bagh. Sci. J.* **8**, 1 (2011).
22. N. Rani and N. Jaggi, *Rad. Phys. Chem.* **201**, 110465 (2022).
23. S. Tajudin, A. A. Sabri, M. A. Aziz, S. Olukotun, B. Ojo, and M. Fasasi, *Nucl. Engin. Tech.* **51**, 1633 (2019).
24. M. Souli, C. Nefzi, Z. Seboui, A. Mejri, R. Vidu, and N. Kamoun-Turki, *Mater. Sci. Semicon. Proces.* **83**, 50 (2018).
25. M. B. A. Bashir, E. Y. Salih, A. H. Rajpar, G. Bahmanrokh, and M. F. M. Sabri, *J. Micromech. Microengin.* **32**, 085006 (2022).
26. N. Papež, A. Gajdoš, R. Dallaev, D. Sobola, P. Sedlak, R. Motuz, A. Nebojsa, and L. Grmela, *Appl. Surf. Sci.* **510**, 145329 (2020).
27. Y. Areerob, C. Hamontree, P. Sricharoen, N. Limchoowong, S. Laksee, W.-C. Oh, and K. Pattarith, *RSC advan.* **12**, 15427 (2022).
28. S. Prayogi and Z. Zainuddin, *Tri Dasa Mega J. Nucl. Reac. Tech.* **25**, 9 (2023).
29. H. Abdullah, H. Al-Taay, M. Khalaf, H. Oleiwi, and A. Rahma, in *Journal of Physics: Conference Series*, IOP Publishing, 2021, p. 012074.
30. S. O. Abdulghani, E. Y. Salih, and A. S. Mohammed, *Mat. Chem. Phys.* **303**, 127859 (2023).
31. B. Bathula, T. R. Gurugubelli, J. Yoo, and K. Yoo, *Catal.* **13**, 765 (2023).
32. N. M. Hadi and K. A. Ammar, in *IOP Conference Series: Materials Science and Engineering*, IOP Publishing, 2020, p. 072101.

33. Z. Zhang, M. Xu, X. Ruan, J. Yan, J. Yun, W. Zhao, and Y. Wang, Ceram. Intern. **43**, 3443 (2017).
34. A. Alhuthali, M. El-Nahass, A. Atta, M. Abd El-Raheem, K. M. Elsabawy, and A. Hassanien, J. Lumin. **158**, 165 (2015).
35. E. Y. Salih, M. B. A. Bashir, A. H. Rajpar, and I. A. Badruddin, Ceram. Intern. **48**, 9965 (2022).
36. S. Kumar, Vacuum **182**, 109725 (2020).
37. C. Ke, W. Zhu, J. Pan, and Z. Yang, Curr. Appl. Phys. **11**, S306 (2011).
38. J. Hassan, Advan. Mat. Res. **1175**, 47 (2023).
39. E. Y. Salih, A. Ramizy, O. Aldaghri, M. F. M. Sabri, N. Madkhali, T. Alinad, K. H. Ibnaouf, and M. H. Eisa, Nanomat. **12**, 1477 (2022).
40. R. Ponte, E. Rauwel, and P. Rauwel, Material, **16**, 4339 (2023).
41. J. Gong, Y. Cui, F. Li, and M. Liu, Small Sci. **3**, 2200108 (2023).
42. V. Kumar, S. K. Sharma, T. Sharma, and V. Singh, Optic. Mat. **12**, 115 (1999).
43. A. Dolgonos, T. O. Mason, and K. R. Poeppelmeier, J. Sol. Stat. Chem. **240**, 43 (2016).
44. T. Kamiya, K. Nomura, and H. Hosono, Phys. Stat. Sol. **206**, 860 (2009).
45. M. Pervez, M. Mia, S. Hossain, S. Saha, M. Ali, P. Sarker, M. K. Hossain, M. Matin, M. Hoq, and M. Chowdhury, Optic. **162**, 140 (2018).
46. J. Mangaiyarkkarasi, V. Meenakumari, and N. Thenmozhi, Sādhanā **48**, 86 (2023).
47. N. K. Abdalameer, Advan. Nat. Appl. Sci. **11**, 357 (2017).
48. K. A. Aadim and M. A. Essa, J. Coll. Educ. **3**, 109 (2019).
49. S. Sarangi, G. K. Pradhan, and D. Samal, J. Allo. Comp. **762**, 16 (2018).
50. R. Narzary, B. Dey, L. Chouhan, S. Kumar, S. Ravi, and S. Srivastava, Mat. Sci. Semicon. Proces. **142**, 106477 (2022).

## دراسة الخصائص التركيبية والبصرية والشكلية للأغشية $\text{SnO}_2$ النانوية تحت تأثير أشعة جاما

علا محمد فراس عبدالله<sup>1</sup> و باسم خلف رجه<sup>1</sup>

<sup>1</sup>قسم الفيزياء، كلية العلوم للبنات، جامعة بغداد، بغداد، العراق

### الخلاصة

تم في هذا البحث دراسة تصنيع أغشية رقيقة من أكسيد القصدير باستخدام تقنية الترسيب بالليزر النبضي. تمت دراسة تأثير إشعاع كاما  $^{60}\text{Co}$  بشكل منهجي على السمات الهيكلية والمورفولوجية والبصرية باستخدام عدة تقنيات تحليبية بما في ذلك حبود الأشعة السينية (XRD) والفحص المجهرى الإلكترونى للانبعاثات الميدانية (FE-SEM) والفحص المجهرى للقوة الذرية (AFM) تحليلاً الأشعة فوق البنفسجية المرئية (UV-Vis). لوحظ أن حجم البلورات قد انخفض من 45.5 إلى 40.8 نانومتر للعينة الأصلية المشعة باستخدام مصدر كاما 1200 جrai من  $^{60}\text{Co}$ . كما أظهر تحليل FE-SEM نتائج مشابهة لتلك التي تم الحصول عليها باستخدام XRD؛ حيث كان قطر الجسيم حوالي 93.8 و 79.9 نانومتر للعينات المشعة المذكورة أعلاه. وعلى الجانب الآخر، لوحظ انخفاض في فجوة النطاق البصري المحسوبة؛ حيث كانت فجوات النطاق البصري تقدر بـ 3.08 و 3.24 فولت للعينة الأصلية المشعة بـ 1200 جrai. بهذه الطريقة، تم توثيق التأثيرات المختلفة للإشعاع على أداء الأغشية الرقيقة المصنوعة من أكسيد القصدير، مما يسهم في فهم أفضل لاستجابتها تحت هذه الظروف وفتح المجال للتطبيقات المحتملة في مجموعة متنوعة من المجالات التقنية والصناعية.

الكلمات المفتاحية:  $\text{SnO}_2$ ، أشعة غاما، ليزر نبضي، ترسيب، خواص.